Springer

KSME

Journal of Mechanical Science and Technology 32 (7) (2018) 3395~3405
www.springerlink.com/content/1738-494x(Print)/1976-3824(Online)
DOI 10.1007/s12206-018-0643-5

Assembly precision prediction for planar closed-loop mechanism in view of joint clearance and redundant constraint †

Qiangqiang Zhao, Junkang Guo* and Jun Hong

Key Laboratory of Education Ministry for Modern Design and Rotor-Bearing System, School of Mechanical Engineering, Xi'an Jiaotong University, Xi'an 710049, China

(Manuscript Received December 27, 2017; Revised March 12, 2018; Accepted March 25, 2018)

Abstract

The assembly process for planar closed-loop mechanisms is full of complexity and uncertainty due to joint clearance, link coupling and probable redundant constraint. In order to ensure assembly precision, an algorithm of predicting accuracy for planar closed-loop mechanisms in view of joint clearance and redundant constraint is proposed. Firstly by analyzing the assembly process of a planar five-bar closed-loop mechanism, three components of single-fixed, two-connected and redundant-inserted links are proposed to describe the assembly process of arbitrary planar closed-loop mechanisms which is regarded as successive stacking of those components. Then error models of those components are established based on the linear kinematics and principle of virtual work. Subsequently, an algorithm of precision prediction for planar closed-loop mechanisms is constructed by combining those error models. Finally the extendible support structure of the SAR antenna is used as the numerical example to verify the validity and generality of the proposed algorithm.

Keywords: Planar closed-loop mechanism; Assembly component; Joint clearance; Redundant constraint; Assembly precision prediction

1. Introduction

In high precision tasks, accuracy is always of the utmost importance. As for planar closed-loop mechanisms, manufacturing tolerance, constraint deviation and joint clearance inevitably lead to position errors of the terminal vertexes of links during the assembly process, resulting in degeneration of the final accuracy of the mechanism [1]. Therefore from the perspective of improving the geometrical precision and implementing accurate assembling adjustment, an effective method of predicting the assembly accuracy is especially critical for planar closed-loop mechanisms to guarantee the assembly quality and performance.

However, planar closed-loop mechanisms possess such complex constraints and interactive couplings that accuracy modeling is more difficult than open-loop mechanisms. And inherent randomness of the joint clearance brings about assembly precision has uncertainty [2-5]. In addition there are two kinds of planar closed-loop mechanisms which are determinate and indeterminate, respectively. Indeterminate closed-loop mechanisms may produce deformation if geometric error exists which leads to the coordinate problem between deformation and geometric error [6]. Hence there are three significant questions to necessarily answer before conducting accuracy prediction for planar closed-loop mechanisms: (1) How to reveal the impact of the complicated coupling among loops on the assembly accuracy; (2) how to analyze the error uncertainty caused by the joint clearance; (3) how to deal with the deformation-error coordinating problem resulted from the geometric errors in the indeterminate closed-loop mechanisms.

Many researchers have been devoted to investigating the effect of manufacturing tolerance and joint clearance on the accuracy of closed-loop mechanisms. Tsai et al. [7] explained why the accuracy of multi-loop linkages is difficult to analyze and they used screw theory to solve the problem. Similarly, Kumaraswamy et al. [8] successfully applied the screw theory to the position error analysis of planar mechanism with considering the joint clearance and link length imperfection. Li et al. [9] studied the angular errors of a multi-loop structure systematically, establishing the explicit solutions of the angular errors with joint clearance and simplifying the extreme error to be an optimization problems based on the invariant rotatability of single-loop linkages. Chebbi et al. [10] developed an analytical predictive model of the pose error for a 3-UPU parallel robot due to joint clearance based on the kinetostatic analysis, and this method can obtain a deterministic result as long as the external force is known. Briot et al. [11] presented the local maximum orientation and position errors of a 3-DOF planar parallel robots considering the input bias according to

*Corresponding author. Tel.: +86 29 83399528, Fax.: +86 29 83399528
E-mail address: guojunkang@gmail.com
† Recommended by Associate Editor Doo Ho Lee

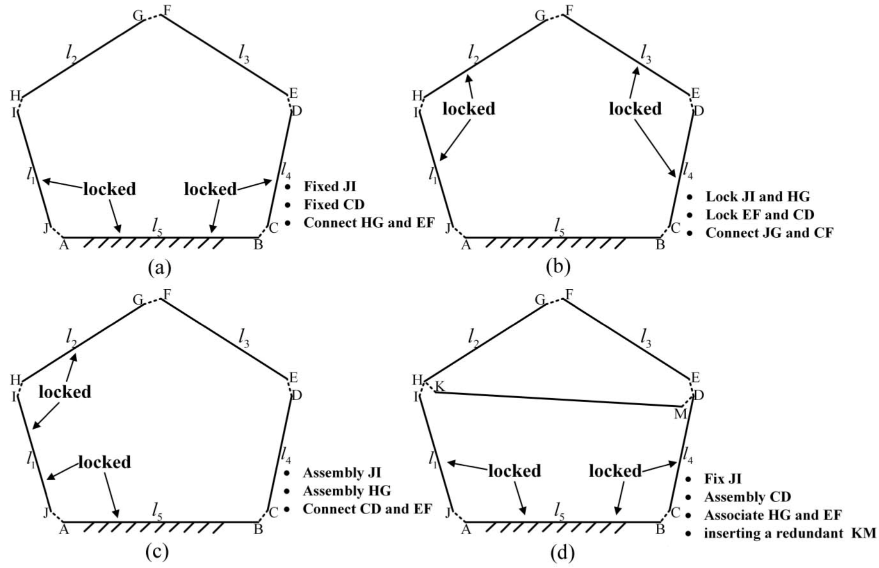

Fig. 1. Assembly process of the planar single-loop five-bar mechanism: (a) Two constraints near the base AB; (b) two constraints away from the base AB; (c) one constraint near the base while the other away from the base; (d) inserting a redundant bar KM.

the interval analysis method. Chen [12] proposed a general method of accuracy analysis for planar parallel mechanisms subjected to errors from the input uncertainties and joints clearance. Besides, plenty of researchers also have studied the kinematic accuracy affected by the joint clearance [13-15] and link imperfection [16, 17]. And a lot of methods are used to deal with the precision problems by the interval approach [18], the matrix method [19], Lie group and Lie algebra method [20], the direct linearization method [21], the level set method [22] and the method based on the generalized kinematic mapping of constrained plane motions [23]. But in contrast fewer literatures [24, 25] involve in the accuracy analysis for closed-loop mechanisms with considering redundant constraints.

It can be seen from above literatures that the previous researches with respect to the accuracy analysis of closed-loop mechanisms focus mostly on the influence of manufacturing errors, joint clearance or input uncertainty on the pose deviation of the end-manipulator or the platform, which still belongs to the field of kinematic accuracy rather than assembly precision. And the common deficiency of methods reviewed above is that they wholly didn’t take account of the manufacturing deviation, joint clearance and redundant constraints simultaneously and meanwhile neglect the indeterminate mechanisms. Many researchers didn’t perform a deep analysis on the deformation-error coordinating problem derived from the redundant constraints so that most methods were only applied to the statically determinate mechanism. As a result many methods of accuracy analysis mentioned above lack generality and are only available for specific mechanisms. Most importantly, few researchers systematically and clearly answered those three key questions about assembly precision prediction for planar closed-loop mechanism.

Therefore, this paper proposes a method of assembly precision prediction for planar closed-loop mechanisms in view of the joint clearance and redundant constraints. Compared with the conventional methods, this method not only takes the joint clearance and redundant constraint into consideration simultaneously but also solves the complex problem of deformation compatibility, which is usually neglected for simplicity in past, by a comparatively simple and intuitive way based on the kinetostatic analysis. And importantly, this method is appropriate for the error modeling of arbitrary planar closed-loop mechanisms regardless of whether the mechanism is indeterminate rather than being only applied to a given closed-loop mechanism.

The contents of this paper are arranged as follows. In Sec. 2, three assembly components are introduced and accordingly their error models are established according to the linear kinematics and principle of virtual work. In Sec. 3, the algorithm of precision prediction for arbitrary planar closed-loop mechanisms is constructed by combining those three error models. In Sec. 4, the proposed method and algorithm are verified by a numerical example of the extendible support structure (ESS) of the SAR antenna which is a three-loop ten-bar mechanism. Finally conclusions and future works are presented in Sec. 5.

2. Error modeling

2.1 Description of assembly process

Assembling planar closed-loop mechanisms is a process of jointing the links, substantially “generating new vertexes”. Fig. 1 illustrates the assembly process of a simply but typical single-loop five-bar mechanism whose DOF is 2, needing two constraints to keep statically determinate. It can be seen from Figs. 1(a)-(c) that the assembly process mainly contains two operations after the reference bar AB is ensured: 1) Create a new vertex by fixing a single bar; 2) generate a new vertex by

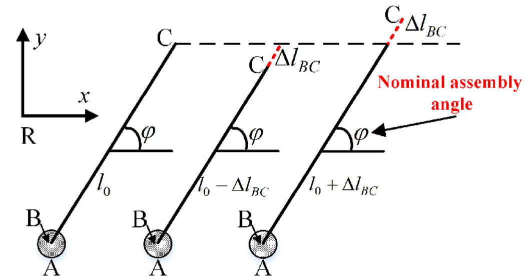

Fig. 2. Single-link assembly component (without considering assembly deviation).

connecting two bars. Those two operations is just subjected to the determinate mechanism. Those two operation are available for all planar closed-loop mechanisms. Besides, the determinate configuration will become indeterminate if adding more constraints or redundant bars to the mechanism as shown in Fig. 1(d). Therefore the conclusion can be drawn that assembly process of arbitrary planar closed-loop mechanisms is realized by fixing single bar, connecting two bars and inserting redundant bar. As a result, the error models of those three assembly operations must be obtained before establishing the assembly prediction algorithm.

2.2 Single-link fixed component

2.2.1 Without assembly deviation

Fig. 2 presents the model of single-link fixed component without considering the assembly deviation. In order to obtain the pose errors of bar BC, the first work is to compute the position error of points B and C. It is readily known that the position error of B results from the base A and the joint clearance between A and B. Therefore the position error of point B can be given by

$$\boldsymbol{\delta}_B^T = \boldsymbol{\delta}_A^T + \boldsymbol{\Gamma}_{AB}^T \tag{1}$$

where $\boldsymbol{\delta}_B$ and $\boldsymbol{\delta}_A$ are respectively the position error of B and A, $\boldsymbol{\Gamma}_{AB}$ represents the joint clearance vector [7] and

$$\begin{cases} \boldsymbol{\delta}_{\mathrm{B}} = [\Delta x_B, \Delta y_B] \\ \boldsymbol{\delta}_A = [\Delta x_A, \Delta y_A] \\ \boldsymbol{\Gamma}_{\mathrm{AB}} = [\Delta x_{AB}, \Delta y_{AB}] \end{cases} \tag{2}$$

where the module of $\boldsymbol{\Gamma}_{AB}$ is not more than the value of the joint clearance. In addition the position misalignment of C is derived from B and the manufacturing error of BC, formulated as

$$\boldsymbol{\delta}_C^T = \boldsymbol{\delta}_B^T + \Delta l_{BC} \boldsymbol{\Phi}_\varphi^T \tag{3}$$

where Δl_{BC} is the length error of BC, $\boldsymbol{\Phi}_\varphi = [\cos\varphi, \sin\varphi]$ and φ is the nominal assembly angle. Substituting Eq. (1) into Eq. (3) gets

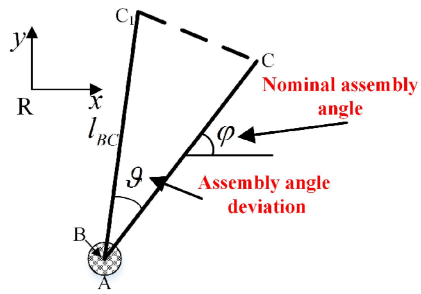

Fig. 3. Single-link assembly component (considering assembly error).

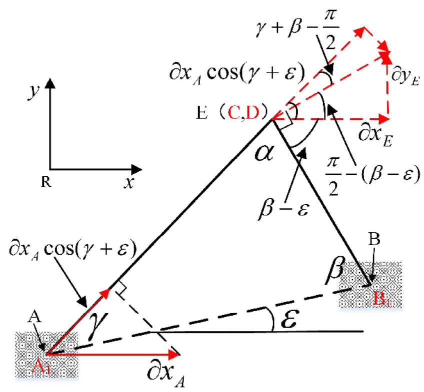

Fig. 4. Schematic sketch for calculating $\partial x_E / \partial x_A$ and $\partial y_E / \partial x_A$ in two-link assembly component.

$$\boldsymbol{\delta}_C^T = \boldsymbol{\delta}_A^T + \boldsymbol{\Gamma}_{AB}^T + \Delta l_{BC} \boldsymbol{\Phi}_\varphi^T . \tag{4}$$

2.2.2 With assembly deviation

Fixing a bar can be divided into two steps when considering the assembly error as depicted in Fig. 3: Firstly assembly BC at the ideal constrained angle φ to create point C; then rotate BC by ϑ (ϑ is the assembly angle error and very small) to produce the final point C_1. Note that the position error of C_1 rather than B is affected by the assembly deviation which is expressed as

$$\begin{cases} \boldsymbol{\delta}_C^T = \boldsymbol{\delta}_A^T + \boldsymbol{\Gamma}_{AB}^T + \Delta l_{BC} \boldsymbol{\Phi}_{\varphi+\vartheta}^T + l_{BC} \vartheta \boldsymbol{\Phi}_{\vartheta/2+\varphi}^T \\ \boldsymbol{\Phi}_{\vartheta/2+\varphi} = [\pm\sin(\frac{1}{2}\vartheta + \varphi), \cos(\frac{1}{2}\vartheta + \varphi)] \\ \boldsymbol{\Phi}_{\varphi+\vartheta} = [\cos(\vartheta + \varphi), \sin(\vartheta + \varphi)] \end{cases} \tag{5}$$

where the first term of $\boldsymbol{\Phi}_{\vartheta/2+\varphi}$, $\pm\sin(\vartheta/2 + \varphi)$, is positive when $\vartheta > 0$ and otherwise is negative.

2.3 Two-link connected component

As shown in Fig. 4, A_1 and B_1 are the bases of AC and BD. Suppose C and D are ideally coincident after connecting AC and BD by initially neglecting the joint clearance between C and D, and the coincident point is denoted as E. Firstly, according to Eq. (1) the position error of A and B can be derived readily as

$$\begin{cases} \boldsymbol{\delta}_A^T = \boldsymbol{\delta}_{A_1}^T + \boldsymbol{\Gamma}_{AA_1}^T \\ \boldsymbol{\delta}_B^T = \boldsymbol{\delta}_{B_1}^T + \boldsymbol{\Gamma}_{BB_1}^T \end{cases}. \tag{6}$$

Then the position deviation of E comes from the base imperfection of A and B and link length errors of AC and BD in terms of Fig. 4, interpreted by

$$\boldsymbol{\delta}_E^T = \boldsymbol{\lambda}_1 \boldsymbol{\Delta}_l^T + \boldsymbol{\lambda}_2 \boldsymbol{\delta}_A^T + \boldsymbol{\lambda}_3 \boldsymbol{\delta}_B^T \tag{7}$$

where $\boldsymbol{\Delta}_l = [\Delta l_{AC}, \Delta l_{BD}]$ and $\boldsymbol{\lambda}_1$, $\boldsymbol{\lambda}_2$, $\boldsymbol{\lambda}_3$ are the Jacobian matrixes defined as

$$\boldsymbol{\lambda}_1 = \begin{bmatrix} \dfrac{\partial x_E}{\partial l_{AC}} & \dfrac{\partial x_E}{\partial l_{BD}} \\ \dfrac{\partial y_E}{\partial l_{AB}} & \dfrac{\partial y_E}{\partial l_{BD}} \end{bmatrix} \tag{8}$$

$$\boldsymbol{\lambda}_2 = \begin{bmatrix} \dfrac{\partial x_E}{\partial x_A} & \dfrac{\partial x_E}{\partial y_A} \\ \dfrac{\partial y_E}{\partial x_A} & \dfrac{\partial y_E}{\partial y_A} \end{bmatrix} \tag{9}$$

$$\boldsymbol{\lambda}_3 = \begin{bmatrix} \dfrac{\partial x_E}{\partial x_B} & \dfrac{\partial x_E}{\partial y_B} \\ \dfrac{\partial y_E}{\partial x_B} & \dfrac{\partial y_E}{\partial y_B} \end{bmatrix}. \tag{10}$$

Therefore $\boldsymbol{\lambda}_1$, $\boldsymbol{\lambda}_2$, $\boldsymbol{\lambda}_3$ should be evaluated before solving Eq. (7). As presented in Fig. 4, point E will rotate around point B by a radius of BD if x_A produces a perturbation ∂x_A while the rest variables keep invariant. Under this circumstances, treat the perturbation ∂x_A as a velocity variable and then we have

$$\begin{cases} \dfrac{\partial x_A \cos(\gamma+\varepsilon)}{\cos(\gamma+\beta-\frac{\pi}{2})} = \dfrac{\partial x_E}{\cos(\frac{\pi}{2}-(\beta-\varepsilon))} \\ \dfrac{\partial x_A \cos(\gamma+\varepsilon)}{\cos(\gamma+\beta-\frac{\pi}{2})} = \dfrac{\partial y_E}{\sin(\frac{\pi}{2}-(\beta-\varepsilon))} \end{cases} \tag{11}$$

where α, β and γ are interior angles of the triangle formed by the two bars and the base structure, detailedly displayed in Fig. 4, and ε is originally the actual angle between the positive direction of axis x and the connecting line of A and B but for simplicity, here ε is the included angle of positive direction of axis x and the base structure of A_1 and B_1. Consequently, $\partial x_E / \partial x_A$ and $\partial y_E / \partial x_A$ are

$$\begin{cases} \dfrac{\partial x_E}{\partial x_A} = \dfrac{\sin(\beta-\varepsilon)\cos(\gamma+\varepsilon)}{\sin\alpha} \\ \dfrac{\partial y_E}{\partial x_A} = \dfrac{\cos(\beta-\varepsilon)\cos(\gamma+\varepsilon)}{\sin\alpha} \end{cases}. \tag{12}$$

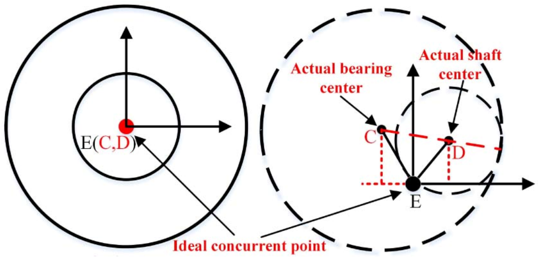

(a) Ideal statement (b) Actual statement

Fig. 5. Actual position of endpoints when connecting two bars.

By making use of the similar mechanisms like Fig. 4, the other independent variables with respect to the position error of E can be figured out as well. Accordingly Jacobian matrixes $\boldsymbol{\lambda}_1$, $\boldsymbol{\lambda}_2$, $\boldsymbol{\lambda}_3$ are identified as

$$\boldsymbol{\lambda}_1 = \begin{bmatrix} \dfrac{\sin(\beta-\varepsilon)}{\sin\alpha} & -\dfrac{\sin(\gamma+\varepsilon)}{\sin\alpha} \\ \dfrac{\cos(\beta-\varepsilon)}{\sin\alpha} & \dfrac{\cos(\gamma+\varepsilon)}{\sin\alpha} \end{bmatrix} \tag{13}$$

$$\boldsymbol{\lambda}_2 = \begin{bmatrix} \dfrac{\sin(\beta-\varepsilon)\cos(\gamma+\varepsilon)}{\sin\alpha} & \dfrac{\sin(\beta-\varepsilon)\sin(\gamma+\varepsilon)}{\sin\alpha} \\ \dfrac{\cos(\beta-\varepsilon)\cos(\gamma+\varepsilon)}{\sin\alpha} & \dfrac{\cos(\beta-\varepsilon)\sin(\gamma+\varepsilon)}{\sin\alpha} \end{bmatrix} \tag{14}$$

$$\boldsymbol{\lambda}_3 = \begin{bmatrix} \dfrac{\cos(\beta-\varepsilon)\sin(\gamma+\varepsilon)}{\sin\alpha} & \dfrac{\sin(\beta-\varepsilon)\sin(\gamma+\varepsilon)}{-\sin\alpha} \\ \dfrac{\cos(\beta-\varepsilon)\cos(\gamma+\varepsilon)}{-\sin\alpha} & \dfrac{\sin(\beta-\varepsilon)\cos(\gamma+\varepsilon)}{\sin\alpha} \end{bmatrix}. \tag{15}$$

Then the introduction of $\boldsymbol{\lambda}_1$, $\boldsymbol{\lambda}_2$ and $\boldsymbol{\lambda}_3$ into Eq. (7) can yield the position error of the concurrent point E.

Nevertheless in fact, C and D maybe not hold together with great probability due to the existence of joint clearance and they will deviate from the concurrent E as shown in Fig. 5. Hence uniting Eqs. (1) and (7), the actual position errors of C and D are given by

$$\begin{cases} \boldsymbol{\delta}_C^T = \boldsymbol{\delta}_E^T + \boldsymbol{\Gamma}_{CE}^T \\ \boldsymbol{\delta}_D^T = \boldsymbol{\delta}_E^T + \boldsymbol{\Gamma}_{DE}^T \end{cases} \tag{16}$$

where $\boldsymbol{\Gamma}_{CE}$ and $\boldsymbol{\Gamma}_{DE}$ are the offset vectors of C and D relative to E. Because of the mating constraint between the shaft and bearing, $\boldsymbol{\Gamma}_{CE}$ and $\boldsymbol{\Gamma}_{DE}$ must satisfy

$$\left|\boldsymbol{\Gamma}_{CE} - \boldsymbol{\Gamma}_{DE}\right| \le r_c \tag{17}$$

where r_c is the magnitude of joint clearance and $|\bullet|$ represents the vector norm.

2.4 Redundant-link inserted component

In general, two cases exist in assembling redundant link. On the one hand, the length of redundant link equals the distance

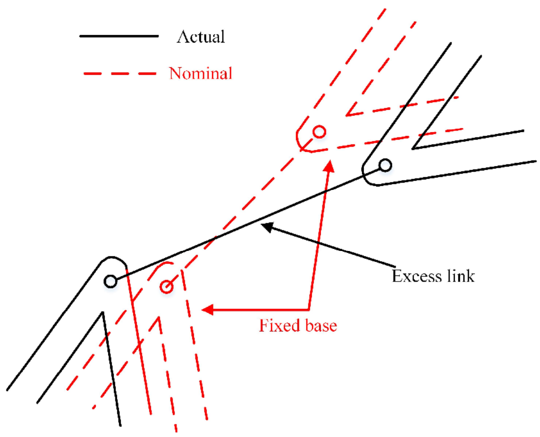

Fig. 6. Actual sketch of inserting a redundant bar.

between two bases and the mechanism keeps stable without deformation; on the other hand, the redundant link has deviation comparing with the two connected bases, unfortunately resulting in deformation inside the bars after inserting it. In this paper the latter case illustrated in Fig. 6 is taken into account and discussed sequentially.

Before solving the problem of inserting redundant bar, the following assumption is given: All bars except the redundant one don't generate deformation when installing it, namely implying the base structure is thought of as a rigid body. Firstly, because the offset between the length of the inserted bar and fixed bases is so small that deformation of the redundant bar can't produce great force on the base structure; on the other hand, the stiffness of the base structure is much bigger in contrast with the redundant bar, indicating the base structure exerted by small force from the redundant bar hardly appear deformation. Therefore the above hypothesis can be truly accessible for practical engineering.

In term of the hypothesis, inserting redundant bar with deviation Δl_r can be identified with implementing forces $\Delta \mathbf{f}_2$ and $-\Delta \mathbf{f}_2$ on the base structure as shown in Fig. 7. The magnitude of $\Delta \mathbf{f}_2$ is

$$|\Delta \mathbf{f}_2| = k\Delta l_r^* \tag{18}$$

which can be rewritten by a vector form for sequent discussion as

$$\Delta \mathbf{f}_2 = [\Delta f_{2x}, \Delta f_{2y}]^T \,. \tag{19}$$

It should be noted that Δl_r^* doesn't equal Δl_r since the position of the base points will change under the force. Equally important, the imposing orders of $\Delta \mathbf{f}_2$ and $-\Delta \mathbf{f}_2$ distinguishes in assembly process. As the one end of the redundant link is jointed to the one fixed base, the force $\Delta \mathbf{f}_2$ is exerted on this base point. And then $\mathbf{cf}_j$ and $-\mathbf{cf}_j$, the contact forces of the shaft and bearing of the joint as shown in Fig. 8, appear under the action of $\Delta \mathbf{f}_2$ and accordingly the mechanism maintains static equilibrium by those forces. Subsequently $-\Delta \mathbf{f}_2$ acts on the other base point and the whole base structure still keeps original equilibrium configuration. In terms of the above analysis, determining the position errors of the endpoints of links when inserting the redundant bar is in essence to obtain the displacement bias under the external force $\Delta \mathbf{f}_2$ (if $-\Delta \mathbf{f}_2$ is applied first, here the external force is $-\Delta \mathbf{f}_2$).

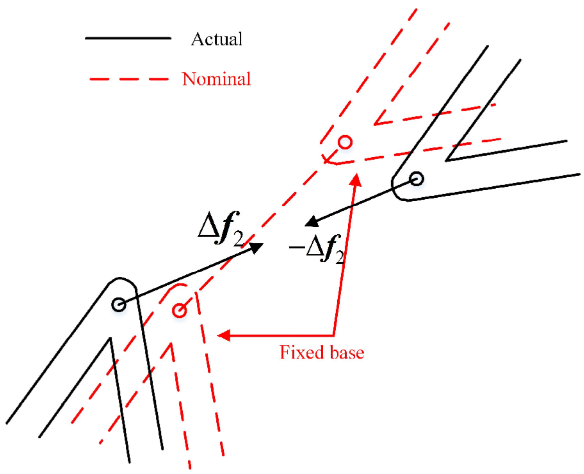

Fig. 7. Equivalent sketch of inserting a redundant bar.

The actual joint generally has clearance but here let the joint be clearance-free. According to the static equilibrium, the contact force in the *j*th joint is

$$\mathbf{cf}_j = \mathbf{s}_j \Delta \mathbf{f}_2 \tag{20}$$

where $\mathbf{f} = \Delta \mathbf{f}_2$ and $\mathbf{s}_j$ is a 2×2 matrix whose elements only depend on the mechanism configuration and $\Delta \mathbf{f}_2$. Next based on the Principle of Virtual work the mechanism of restoring equilibrium satisfies the following equation

$$\sum \mathbf{f} \bullet \delta \mathbf{r} = 0 \,. \tag{21}$$

Accordingly applying the principle to the base structure free of joint clearance in Fig. 7 can obtain

$$\begin{aligned}(cf_{jx}\delta cp_{ajx} + cf_{jy}\delta cp_{ajy} - cf_{jx}\delta cp_{bjx} \\ -cf_{jy}\delta cp_{bjy}) + \Delta f_{2x}\delta_{fx} + \Delta f_{2y}\delta_{fy} = 0\end{aligned} \tag{22}$$

where cf_{jx} and cf_{jy} are the contact forces of the *j*th joint, δcp_{ajx}, δcp_{ajx}, δcp_{bjx} and δcp_{bjx} are the virtual displacements of the two contact points a and b as presented in Fig. 8 along the directions of axis *x* and *y*, respectively. Rewrite Eq. (22) by the vector format as

$$(\mathbf{cf}_j \delta \mathbf{cp}_{aj} - \mathbf{cf}_j \delta \mathbf{cp}_{bj}) + \Delta \mathbf{f}_2 \delta \mathbf{r}_f = 0 \,. \tag{23}$$

It's readily known from Fig. 8 that

$$\delta \mathbf{cp}_j = \delta \mathbf{cp}_{aj} - \delta \mathbf{cp}_{bj} . \tag{24}$$

Then substituting Eqs. (20) and (24) into Eq. (23) gets

$$\Delta \mathbf{f}_2 \bullet \delta \mathbf{\Gamma} + \mathbf{s}_j \Delta \mathbf{f}_2 \bullet \delta \mathbf{cp}_j = 0 . \tag{25}$$

Simplify the above equation as

$$\delta \mathbf{\Gamma} = -\mathbf{s}_j \bullet \delta \mathbf{cp}_j \tag{26}$$

where

$$\delta \mathbf{cp}_j = \delta cp_j \frac{\mathbf{cf}_j}{|\mathbf{cf}_j|} . \tag{27}$$

It is seen from Eq. (27) that the influence of joint clearance on the position error of the acting point is not relevant with the magnitude of the force. Given the base structure owns more than one joint, the position error of the acting point

$$\delta \mathbf{\Gamma} = \sum_{j=1}^{n} -\mathbf{s}_j \bullet \delta \mathbf{cp}_j \tag{28}$$

where n is the joint number. Substitute Eq. (27) into Eq. (28) and we obtain

$$\delta \mathbf{\Gamma} = \sum_{j=1}^{n} -\delta cp_j \mathbf{s}_j \bullet \frac{\mathbf{cf}_j}{|\mathbf{cf}_j|} . \tag{29}$$

Generally speaking, the joint clearance can be treated as infinitesimal because it is much smaller relative to the nominal length of bars, consequently

$$\delta \mathbf{cp}_j = \Delta \mathbf{cp}_j = r_{cj} \frac{\mathbf{cf}_j}{|\mathbf{cf}_j|} \tag{30}$$

where r_{cj} is the value of the jth joint clearance. Then the introduction of Eq. (30) into Eq. (29) leads to the equation

$$\delta \mathbf{\Gamma} = \sum_{j=1}^{n} -r_{cj} \mathbf{s}_j \bullet \frac{\mathbf{cf}_j}{|\mathbf{cf}_j|} . \tag{31}$$

In the meantime considering the two forces respectively applied on the shaft and bearing are reaction, the virtual displacements of their centers equal but possess opposite directions, which signifies

$$\delta \mathbf{cp}_{aj} = -\delta \mathbf{cp}_{bj} . \tag{32}$$

Uniting Eqs. (24), (30) and (32) generates

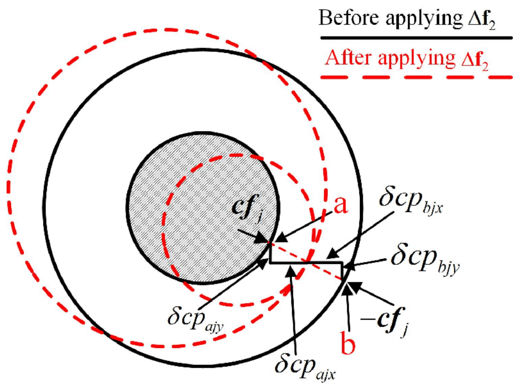

Fig. 8. Sketch of virtual displacement of the jth joint clearance as the mechanism applied by $\Delta \mathbf{f}_2$.

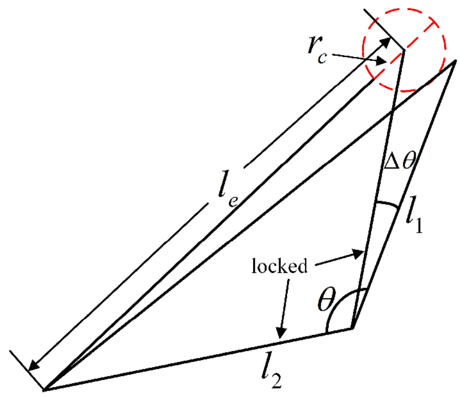

Fig. 9. Open-chain generalized link.

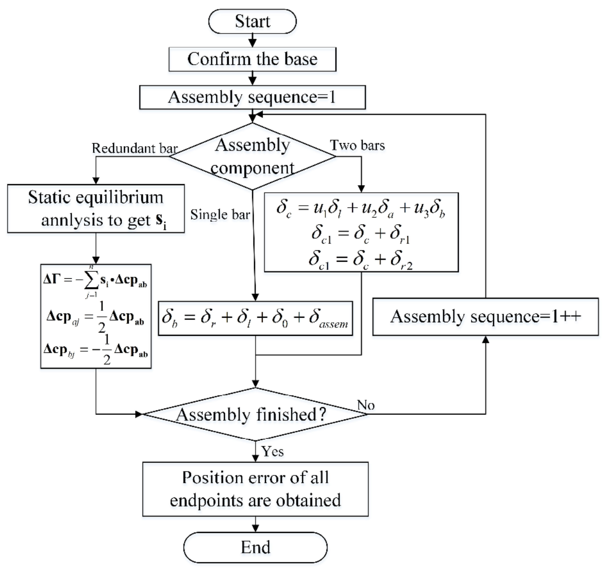

Fig. 10. Algorithm of assembly precision prediction for planar closed-loop mechanisms.

$$\Delta \mathbf{cp}_{aj} = -\Delta \mathbf{cp}_{bj} = \frac{1}{2} \Delta \mathbf{cp}_{ab} = \frac{1}{2} r_{cj} \frac{\mathbf{cf}_j}{|\mathbf{cf}_j|} . \tag{33}$$

Accordingly the position errors of the endpoints, i.e. the centers of the shaft and bearing, can be calculated by Eqs. (33) and (31) when assembling a redundant link. Then the actual assembly errors of links are able to be obtained by superposition with the original error of the base structure before inserting the redundant bar. But it should be noted that the mentioned 'original error' above should be evaluated without taking account of the joint clearance.

Table 1. Structure parameters of the ESS.

Bars	Nominal value (mm)	Deviation (mm)
AF	212	1.10
DF	93	-0.75
ED	218.71	0.94
FI	210	-1.26
DI	229.67	-0.86
AB	125	0.94
BD	214.4	1.03
AE	14	-0.35

Table 2. Errors of 90- and 180-degree locked joints.

Antenna panels	Angle error (°)	Local angle (°)
AF (inner panel)	-1.26	-210
FI (outer panel)	0.95	60

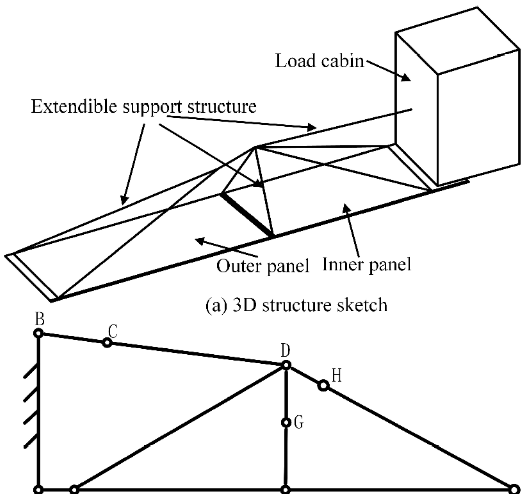

(a) 3D structure sketch

(b) Planar projected model

Fig. 11. The ESS of the planar SAR antenna (planar three-loop mechanism with ten bars).

2.5 Generalized link

Three abovementioned assembly components all involve in 'single link'. This 'single link' is defined as a generalized link which represents not only the actual single bar but also multi-bar subassembly. Thus the generalized link probably possesses 'length deviation' due to the manufacturing imperfection, joint clearance and assembly error as well.

Fig. 9 shows a simply generalized bar consisted of two bars. Without considering the joint clearance, the length of equivalent link is

$$l_{e0} = \sqrt{l_1^2 + l_2^2 - 2l_1 l_2 \cos(\theta - \Delta\theta)} \tag{34}$$

where l_1 and l_2 is the actual length, $\Delta\theta$ is the constraint error between two bars.

The clearance vector can rotate by 360 degrees. Therefore translate the clearance vector to the end of equivalent link according to the parallelogram rule and as a result the actual length of the equivalent link with clearance is expressed as

$$l_e = \sqrt{l_{e0}^2 + r_c^2 - 2l_{e0} r_c \cos\varsigma} \tag{35}$$

where ς is the angle of clearance vector in the local frame and r_c is the joint clearance. Thus the minimum and maximum value respectively are

$$\begin{cases} l_{e\min} = l_e - r_c \\ l_{e\max} = l_e + r_c \ . \end{cases} \tag{36}$$

By parity of reasoning, The minimum and maximum equivalent length of a n-bar open-chain generalized bar can be derived from Eq. (36) as

$$\begin{cases} l_{e\min} = \left| \vec{l}_1 + \vec{l}_2 + \cdots + \vec{l}_n \right| - (n-1) r_c \\ l_{e\max} = \left| \vec{l}_1 + \vec{l}_2 + \cdots + \vec{l}_n \right| + (n-1) r_c \ . \end{cases} \tag{37}$$

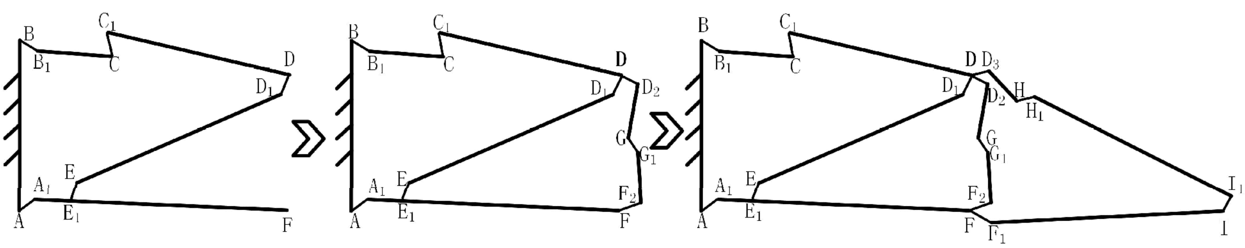

Fig. 12. Assembly process of over-constrained ESS.

3. Algorithm of assembly precision prediction

In Sec. 2, error models for three assembly components of planar closed-loop mechanisms have been established. At present, we are ready to use those three models within a whole algorithm so as to calculate the position errors generated during the assembly process. This algorithm depicted in Fig. 10 are divided into four steps:

Step 1: Determine the base bar to be the reference of the whole mechanism in assembly process;

Step 2: Judge the operation type of this assembly sequence and then conduct the proper calculations of the position error in term of those three models;

Step 3: Implement the next-sequence assembling operation and continue to repeat the step 2;

Step 4: Recycle the steps 2 and 3 until the mechanism is assembly completely and all the position errors of the points are obtained.

4. Results and discussion

The ESS of the SAR antenna (a planar three-loop mechanism with ten bars), whose structure is presented in Fig. 11, will be the numerical example to demonstrate the utility of the above algorithm. In general the ESS is a structure with redundant constraint in actual assembly process. However for lowering the analysis difficulty, the over-constraint ESS was ever-simplified to a statically determinate structure [9]. Now without loss of generality, those two cases both are to be analyzed in this paper.

4.1 Over-constraint ESS

In Fig. 11, joints C, G and H are all 180-degree locked joints which will guarantee the angle between the two bars connected by them being 180 degrees after locked completely and accordingly there are three generalized links BD, DI and DF. Meanwhile joint A is a 90-degree locked joint which attaches the antenna panel AF to the load cabin and two antenna panels are associated with the 180-degree locked joint F. The whole ESS is over-constraint because the constraints are more than the DOFs (the ESS has 5 constraints and 3 DOFs). The concrete structure parameters are presented in Table 1. It should be noted that for simplicity the equivalent lengths and deviations of three generalized bars, which can be evaluated by the Sec. 2.5, are directly given in Table 1. And Table 2 gives the locked angle errors (assembly errors) and the rotation angles of clearance vectors of joints A and F in local framework (note that the rotation angle in local framework is a constant after the joint is locked). Besides all the joint clearances are 0.5 mm.

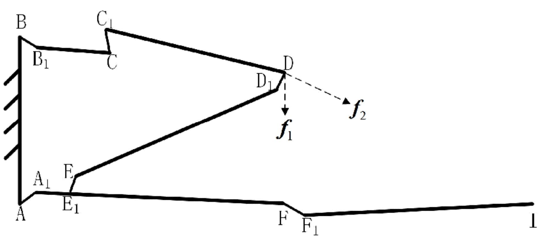

Fig. 13. Equivalent diagram of inserting generalized bars F_1D_2 and I_1D_3.

In the shop floor, the load cabin AB is the reference base and the practical assembly sequences of over-constraint ESS are shown in Fig. 12.

Sequence 1: Assembly the single bar A_1F (the inner panel) attached to the load cabin by a 90-degree locked joint;

Sequence 2: Connect the generalized bar B_1D (generated by B_1C and C_1D) and the single bar E_1D_1;

Sequence 3: Insert the redundant generalized bar F_1D_2 (formed by F_1G_1 and GD_2);

Sequence 4: Fix single bar F_2I (the outer panel);

Sequence 5: Install the redundant generalized bar I_1D_3 (formed by I_1H_1 and H_1D_3).

According to the precision prediction algorithm presented in Fig. 10, the assembling position errors of the endpoints of all links in every aforesaid assembly sequences can be readily evaluated. Note that there is a two-bar connected operation in Sequence 2 and based on the Sec. 2.3, the Jacobian matrixes are

$$\boldsymbol{\lambda}_1 = \begin{bmatrix} 1.739 & -1.781 \\ 0.471 & 0.269 \end{bmatrix} \tag{38}$$

$$\boldsymbol{\lambda}_2 = \begin{bmatrix} 0.260 & 1.720 \\ -0.07 & 0.465 \end{bmatrix} \tag{39}$$

$$\boldsymbol{\lambda}_3 = \begin{bmatrix} 0.465 & -1.720 \\ -0.07 & 0.259 \end{bmatrix}. \tag{40}$$

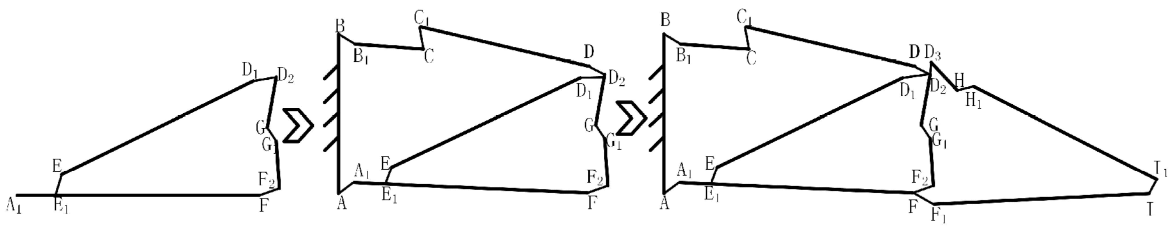

Fig. 14. Assembly process of statically determinate ESS.

Table 3. Assembly position errors of over-constrained ESS.

Endpoints	Position error (mm)
A	(0,0)
A_1	(0.433,0.250)
B	(0,1.100)
B_1	(-0.989,1.249)
D	(-0.658,1.930)
D_1	(-0.388,3.083)
E	(-0.631,0.456)
E_1	(-1.536,-0..033)
F	(-4.019,-0.173)
F_1	(-3.769,0.606)
I	(0.790,0.730)

In Sequences 3 and 5, two redundant generalized bars are inserted and Fig. 13 gives the equivalent schematic diagram. According to Sec. 2.4, the contact-force matrixes of clearance-free joints B, E and D applied by $\mathbf{f}_1$ are

$$\begin{cases} \mathbf{s}_{1B} = \begin{bmatrix} -1.611 & 0 \\ 0 & 0.243 \end{bmatrix} \\ \mathbf{s}_{1E} = \begin{bmatrix} 1.611 & 0 \\ 0 & 0.757 \end{bmatrix} \\ \mathbf{s}_{1D} = \begin{bmatrix} 0 & 0 \\ 0 & 1 \end{bmatrix}. \end{cases} \tag{41}$$

And at the same time the contact-force matrixes exerted by $\mathbf{f}_2$ are calculated as

$$\begin{cases} \mathbf{s}_{2B} = \begin{bmatrix} -1.44 & 0 \\ 0 & 0.51 \end{bmatrix} \\ \mathbf{s}_{2E} = \begin{bmatrix} 0.44 & 0 \\ 0 & 0.49 \end{bmatrix} \\ \mathbf{s}_{2D} = \begin{bmatrix} 0.92 & 0 \\ 0 & 0.39 \end{bmatrix}. \end{cases} \tag{42}$$

Substitute those Jacobian matrixes, contact-force matrixes and the related parameters into the error models and accordingly the precision can be predicted in assembly process so as to guide the workers to adjust the accuracy in assembly shop of the ESS. In addition the results of all position errors are presented in Table 3.

4.2 Statically determinate ESS

Different from the over-constrained ESS, the 90- and 180-degree locked joints of A and F of the statically determine ESS as shown in Fig. 14 become free for the purpose of simplicity. The assembly sequences for the statically determine ESS shown in Fig. 14 are elaborated as following:

Sequence 1: Let the inner panel A_1F be the base bar and connect the generalized bar D_2F_2 (formed by D_2G and G_1F_2) and D_2E, generating a closed-chain generalized bar A_1D_2;

Sequence 2: Joint generalized links A_1D_2 and B_1D (fixed by B_1C and C_1D);

Sequence 3: Associate generalized bar D_3I_1 (locked by D_3H and H_1I_1) and the outer panel F_1I.

It's obviously seen that the assembly process of statically determine ESS differs from the over-constrained one and just involves in the equivalence of generalized links in Sec. 2.5 and two-bar connecting in Sec. 2.3. Similarly the assembling errors can be calculated according to the precision prediction algorithm. And because how to evaluate the position errors has been demonstrated entirely in Sec. 4.1, the concrete error calculating for statically determine ESS will not be displayed once again in case of repetition.

5. Conclusions

Assembly precision prediction for planar closed-loop mechanisms in view of joint clearance and redundant constraints is investigated systematically in this paper. Firstly the assembly process of arbitrary planar closed-loop mechanisms is described by successive stack of three proposed assembly components, which are single-link fixed, two-link connected and redundant-link inserted components. Then the error models of those three components are established and chief of among them, the most difficult problem of assembling precision with redundant constraints is solved based on the principle of virtual work. Subsequently the prediction algorithm of the assembly precision is derived from the combination of the abovementioned error models and moreover calculating the position errors of each assembling sequence is realized for planar closed-loop mechanisms by this algorithm. Finally the prediction algorithm is verified by evaluating the assembly error of the ESS of the SAR antenna.

Compared with the previous methods of accuracy analysis, the advantages of the algorithm proposed in this paper is not only considering all factors influencing the precision including manufacturing deviation, joint clearance and redundant constraints but also available to all planar closed-loop mechanisms. Furthermore the modeling procedures and relevant methods can be expanded to accuracy analysis of spatial closed-loop mechanisms. Therefore our subsequent research will focus more on exploring the algorithm of precision prediction for spatial closed-loop mechanisms.

But meanwhile it should be noted that the assumption in Sec. 2.4 for solving the problem of inserting a redundant link is adequately true only when the components in the mechanism possess good stiffness, indicating the obtained results of position errors based on the above assumption will become inaccurate if stiffness of the links is too small. Hence, for utmost exactitude and covering all closed-loop mechanisms with different flexibility, our follow-up work will also concentrate on the error-deformation coordination problem in view of deformation existing in all bars apart from extending the methods of this paper to the spatial mechanisms.

Acknowledgments

This work is supported by the key project of the National Natural Science Foundation of China (Grant No. 51635010) and the advanced project about Sharing Technology for Equipment of the Equipment Development Department of China (Grant No. 41423010401).

References

[1] C. Innocenti, Kinematic clearance sensitivity analysis of spatial structures with revolute joints, *Journal of Mechanical Design*, 124 (1) (2002) 52-57.
[2] Y. Yang et al., Accuracy model, analysis, and adjustment in the context of multi-closed-loop planar deployable mechanisms, *Advances in Mechanical Engineering*, 8 (3) (2016) 1-15.
[3] J. Meng and Z. Li, A general approach for accuracy analysis of parallel manipulators with joint clearance, *IEEE/RSJ International Conference on Intelligent Robots and Systems, IEEE* (2005) 2468-2473.
[4] K. L. Ting, J. Zhu and D. Watkins, The effects of joint clearance on position and orientation deviation of linkages and manipulators, *Mechanism & Machine Theory*, 35 (3) (2000) 391-401.
[5] A. Frisoli, M. Solazzi and M. Bergamasco, A new method for the estimation of position accuracy in parallel manipulators with joint clearances by screw theory, *IEEE International Conference on Robotics and Automation, IEEE* (2008) 837-844.
[6] S. Erkaya and S. Doğan, A comparative analysis of joint clearance effects on articulated and partly compliant mechanisms, *Nonlinear Dynamics*, 81 (1-2) (2015) 323-341.
[7] M. J. Tsai and T. H. Lai, Accuracy analysis of a multi-loop linkage with joint clearances, *Mechanism & Machine Theory*, 43 (9) (2008) 1141-1157.
[8] U. Kumaraswamy, M. S. Shunmugam and S. Sujatha, A unified framework for tolerance analysis of planar and spatial mechanisms using screw theory, *Mechanism & Machine Theory*, 69 (6) (2013) 168-184.
[9] X. Li, X. L. Ding and G. S. Chirikjian, Analysis of angular-error uncertainty in planar multiple-loop structures with joint clearances, *Mechanism & Machine Theory*, 91 (2015) 69-85.
[10] A. H. Chebbi, Z. Affi and L. Romdhane, Prediction of the pose errors produced by joints clearance for a 3-UPU parallel robot, *Mechanism & Machine Theory*, 44 (9) (2009) 1768-1783.
[11] S. Briot and I. A. Bonev, Accuracy analysis of 3-DOF planar parallel robots, *Mechanism & Machine Theory*, 43 (4) (2008) 445-458.
[12] G. Chen, H. Wang and Z. Lin, A unified approach to the accuracy analysis of planar parallel manipulators both with input uncertainties and joint clearance, *Mechanism & Machine Theory*, 64 (6) (2013) 1-17.
[13] Z. F. Bai, Y. Q. Liu and Y. Sun, Investigation on dynamic responses of dual-axis positioning mechanism for satellite antenna considering joint clearance, *Journal of Mechanical Science & Technology*, 29 (2) (2015) 453-460.
[14] Y. Chen, Y. Sun and D. Yang, Investigations on the dynamic characteristics of a planar slider-crank mechanism for a high-speed press system that considers joint clearance, *Journal of Mechanical Science & Technology*, 31 (1) (2017) 75-85.
[15] B. Xu et al., Dynamic and motion consistency analysis for a planar parallel mechanism with revolute dry clearance joints, *Journal of Mechanical Science & Technology*, 31 (7) (2017) 3199-3209.
[16] D. Sun and G. Chen, Kinematic accuracy analysis of planar mechanisms with clearance involving random and epistemic uncertainty, *European Journal of Mechanics - A/Solids*, 58 (2016) 256-261.
[17] Y. Cai, B. Zhang and Y. Yao, Kinematics accuracy and reliability analysis for 3PTT-2R series-parallel mechanism, *Prognostics and System Health Management Conference,* IEEE (2014) 499-503.
[18] W. Wu and S. S. Rao, Interval approach for the modeling of tolerances and clearances in mechanism analysis, *Journal of Mechanical Design*, 126 (4) (2004) 581-592.
[19] P. D. Lin and J. F. Chen, Accuracy analysis of planar linkages by the matrix method, *Mechanism & Machine Theory*, 27 (5) (1992) 507-516.
[20] J. Meng, D. Zhang and T. Zhang, Accuracy Analysis of general parallel manipulators with joint clearance, *International Conference on Robots and Automation, IEEE* (2007) 889-894.
[21] J. W. Wittwer, K. W. Chase and L. L. Howell, The direct linearization method applied to position error in kinematic linkages, *Mechanism & Machine Theory,* 39 (7) (2004) 681-693.
[22] H. Wang, G. Chen and Y. Zhao, Output error bound prediction of parallel manipulators based on the level set method, *Mechanism & Machine Theory*, 45 (8) (2010) 1153-1170.
[23] G. Chen, H. Wang and Z. Lin, Generalized kinematic mapping of constrained plane motions and its application to the accuracy analysis of general planar parallel robots, *Mechanism & Machine Theory*, 50 (2) (2012) 29-47.
[24] J. Meng, D. Zhang and Z. Li, Assembly problem of over-constrained and clearance-free parallel manipulators, *IEEE International Conference on Robotics and Automation, IEEE* (2007) 1183-1188.
[25] S. R. Lim, K. Kang and S. Park, Error analysis of a parallel mechanism considering link stiffness and joint clearances, *KSME International Journal*, 16 (6) (2002) 799-809.

Qiangqiang Zhao received his B.S. degree from Xi'an Jiaotong University, Shaanxi, China, in 2015. He is currently a doctoral candidate in School of Mechanical Engineering of Xi'an Jiaotong University. His major area is the error modeling and kinematic reliability analysis of the multi-loop mechanism with link flexibility and joint clearance.

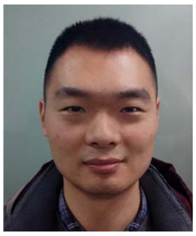

Junkang Guo recived his Ph.D. degree from School of Mechanical Engineering of Xi'an Jiaotong University, Shaanxi, China, in 2017, and worked as a Visiting Scholar in Graduate School of Engineering Department of Micro Engineering, Kyoto University, Japan, during 2015-2016. Currently, he is an Assistant Researcher at Xi'an Jiaotong University. His major interests are accuracy design of the mechanical system, assembly quality assurance, digital assembly, etc.

Jun Hong received his M.S. and Ph.D. degrees from School of Mechanical Engineering of Xi'an Jiaotong University, Shaanxi, China, in 1994 and 2001, respectively. He is currently a Professor in School of Mechanical Engineering of Xi'an Jiaotong University, where he also is the Principal Assistant. In 2014, he was a Distinguished Professor of Yangtze River Scholar of the Chinese Ministry of Education. His research interests include precision assembly, topological optimization design, modeling and analysis of the high-speed precision spindle, etc.